Extended Defects Created By Light Ion Implantation In Germanium

M.L. David[a], J. F. Barbot[a], S. Rousselet[a], F. Pailloux[a], D. Babonneau[a], MF. Beaufort[a],
L. Pizzagalli[a], M. Drouet[a], E. Simoen[b] and C. Claeys[b,c]

[a] PHYMAT, Université de Poitiers/CNRS, UMR 6630, bd M&P Curie, BP 30179, 86962
Futuroscope-Chasseneuil cedex, France
[b] IMEC, Kapeldreef 75, B-3001 Leuven, Belgium
[c] E.E. Dept., KU Leuven, Kasteelpark Arenberg 10, B-3001 Leuven, Belgium

The effect of the implantation temperature in the range room temperature − 300°C has been studied in hydrogen and helium implanted germanium at high fluence and in the energy range of few tens of keV with either conventional implantation or plasma based ion implantation. The microstructure of the as-implanted Ge samples has been studied by Grazing Incidence Small-Angle X-ray Scattering and/or Transmission Electron Microscopy. For H-implanted Ge, small (001) and {111} platelets and {113} defects are nucleated at RT. With increasing the implantation temperature, microcracks, cavities and plate-like cavity clusters are created as well. The formation of these types of defects is ascribed to the interplay between dynamic and kinetic effects occurring during the implantation. As for He implanted Ge, a continuous cavity layer is formed whatever the implantation temperature in the range studied.

Introduction

Light ion implantation in semiconductors has found numerous technological applications. For instance, one of the most famous is probably the implantation of H in Si which is used in the frame of the smart cut[TM] process to produce Silicon On Insulator (SOI) wafers (1). Since then, the layer splitting process via ion cutting has been demonstrated in many other semiconductors such as SiC, diamond, InP, GaAs or Ge (2-5). Nowadays, H and He co-implantation is used in the SOI technology to lower the fluence needed for layer splitting (6 and references therein). On the other hand, as an attractive process to engineer the material properties via the as-created defects, ion implantation still constitutes a substantial scientific challenge. As an example, the possibility to use ion cutting to transfer thin layers onto flexible substrates has been explored recently in the case of InP (7). Further, the cavities induced by high fluence He implantation could find potential applications in the annihilation of dislocations in GaN (8), in reducing the threading dislocation density via the enhancement of the strain relaxation of SiGe/Si heterostructures (9) or in the proximity gettering of metallic impurities in Si (10-12). H-related cavities have also been found to be efficient Cu gettering center in multicrystalline Si (13).

In the last decade, defect engineering has triggered many studies on light ion implantation induced defects in semiconductors. However, most of the studies have been devoted to Si; two reviews have been published so far, one dealing with He implantation

(14) and a more recent one with H implantation (6). For instance, in the case of H implantation, these significant efforts have led to the understanding of some of the physical aspects of H-related extended defects, the so-called platelets that are at the origin of the ion cutting process. The H-platelets thermal behavior is now well understood (15) and it has been recently established that their habit plane is dependent on the strain field (16-18). However, some key points such as their atomic structure are still unclear and only controversial literature could be found on this topic (19-25), one of the key points being whether vacancies are involved in the defect structure.

To get a fundamental understanding of the physical processes involved in the defect formation during implantation, the implantation temperature is one of the key issues. The increase of implantation temperature reduces the lattice damage and therefore the stress as well as it enhances the mobilities of the different species. The effect of the implantation temperature in light ion implanted semiconductors has been studied in different materials (26-33). In He-implanted Si, with increasing implantation temperature, concurrently interstitial-type defects lying on {113} planes (rod-like and ribbon-like defects) appear in the region of ion end of range (28,29). In He-implanted SiC where implantation at high temperature avoids the amorphization, small bubbles, lying along rows in the basal plane, form in the highly damaged region (34,35). In general, beyond a threshold temperature, no cavities form (28).

Ge attracts an increasing attention due to its potential use for sub-22 nm Complementary Metal-Oxide-Semiconductor (CMOS) technology owing to the high electron and hall mobility (36), so that nowadays, many studies focus on H implantation or diffusion in Ge, the most puzzling question being whether H behaves in Ge as in Si. The microstructure of a Room Temperature (RT) H-implanted sample annealed at 280°C has revealed that contrary to Si, not only platelets but also bubbles are formed (37). Moreover Raman spectroscopy studies of hydrogenated samples have suggested that the platelet structure depends on the substrate temperature (38). Actually, the GeH and H_2 Raman signals are completely different in the RT-150°C temperature range; both signals disappear for implantation temperature higher than 200°C. Moreover, the importance of the implantation temperature has recently been shown for both low implantation temperature by Raman spectroscopy (33) and high implantation temperature by TEM (31) as compared to RT. On the contrary, He implantation in Ge has received little attention and only few papers deal with this topic (39, 40).

In this paper, the effects of light ion implantation in Ge and more specifically the effects of the implantation temperature in the range RT-300°C are investigated by TEM and Grazing Incidence Small Angle X Ray Scattering (GISAXS). H has been implanted either by conventional implantation or by Plasma Based Ion Implantation (PBII). PBII is an other way to incorporate H in materials. The interest for this technique lies in a relatively simple and low cost instrumentation and cleavage at a specific depth has been demonstrated in Si (41). The main drawback is the lack of selectivity in energy and mass of the implanted species. However, the implanted ion species can be selected by adjusting the plasma conditions, e.g. hydrogen gas pressure, microwave or radio frequency power and magnetic field. The behaviour of H implanted Ge is discussed in the light of He implanted Ge. Whenever possible, the results are compared to what has been observed in light ion implanted Si in the same conditions. Finally, in a more general framework, extended defect formation related to light ion implantation in Ge is compared to Si.

Experiments

(001) n-type Ge samples with a net shallow dopant concentration of $1x10^{16}$ Sb/cm^3 from UMICORE were implanted with hydrogen or helium at a given fluence of $5x10^{16}$ cm^{-2} and in the energy range 20 kV – 50 kV. The implantations have been carried out using either a PBII equipment or a conventional implanter at different temperatures in the RT-300°C range, set by a furnace. For PBII experiments, due to the high current (mean current: 4.2 A) used and the plasma heating, the sample temperature should reach a much higher value than that set by the furnace during the process. We will thus consider that the implantation temperature was higher or equal to that set by the furnace. As for conventional implantations, the current being rather low, we will consider that the temperature did not increase during the implantation process. Table I summarizes the whole set of implantation conditions.

The implantation-induced damage was studied by conventional or High Resolution Transmission Electron Microscopy (respectively TEM or HRTEM) using a JEOL 3010 (300 kV, LaB$_6$, 0.19 nm point resolution) and a JEOL 2200 FS (200 kV, FEG, 0.23 point resolution) microscope. The TEM-samples were prepared in the cross-section geometry; the samples were mechanically thinned using a tripod polisher down to 10 μm and ion milled in a GATAN-PIPS apparatus at low energy (2.5 keV Ar) and low incidence (±8°) to minimize irradiation damage.

GISAXS experiments were also performed on the conventional H-implanted samples at the European Synchrotron Radiation Facility (ESRF) on the D2AM beam line with the incident X-ray beam (wavelength λ = 0.141 nm, grazing angle α_i = 0.55°) oriented along the Ge [110] direction. More details on the GISAXS experiments are given elsewhere (30,42).

In specific cases, the results have been compared with those obtained after similar implantations (same implanter, energy, fluence, current) in Si (28,29).

TABLE I. Implantation conditions used in this study. The projected range and straggling calculated using SRIM 2006 (43) are also added. More details on the PBII experiments are given in (44).

		Energy of atomic hydrogen (keV)	Mean current (A)	R_P (nm)	ΔR_P (nm)	Temperature of implantation
PBII	**H$^+$ (20 kV)**	20 keV		169	55	≥ 150°C, ≥ 300°C
	H$_2^+$ (20 kV)	10 keV	4.2	94	39	
	H$_3^+$ (20kV)	6.6 keV		68	30	
Conventional Implantation	**H$_2^+$ (30kV)**	15 keV	4x10^{-6}	133	48	RT, 150°C
Conventional Implantation	**He$^+$ (50kV)**	50 keV	30x10^{-6}	280	100	RT, 200°C

Results

Hydrogen implantation

Conventional implantation. The two-dimensional GISAXS patterns of Ge samples implanted at RT and at 150°C are shown in Figures 1 a) and b) respectively. As seen, the GISAXS patterns are strongly affected by the implantation temperature. After RT implantation, diffuse rods oriented at 54.7° with respect to the surface normal (corresponding to <111>* directions) are observed, revealing the presence of anisotropic

objects in the {111} planes (30). In the following, defects located in the {xxx} planes, will be noted {xxx} defects. The intense signal in the [001]* direction ($q_y = 0$) could be attributed to the surface roughness or to the presence of defects lying in the (001) plane (31). After a 150°C implantation, the rods in the <111>* directions are more intense and sharper showing that the anisotropic objects in the {111} planes are much extended in the {111} planes. The signal observed in the [001]* direction is also much more intense with increasing the implantation temperature, it is attributed to anisotropic objects lying in the (001) plane (31). In addition, a shoulder appears at 25.2° with respect to the surface normal, that corresponds to the <113>* directions and highlights the presence of nanometric {113} defects (30). Note that in the RT implanted sample, the lack of signal at 25.2° does not exclude the presence of {113} defects; it can indeed be hidden by the signal due to the surface roughness.

For comparison, the GISAXS pattern of a (001) n-type Si sample implanted at RT in the same conditions is shown in Figure 1c. As seen, the patterns of both materials are roughly similar. However, in the H-implanted Si sample, the diffuse rods in the <111>* direction are less intense, suggesting that the defects located in the {111} planes are either smaller and/or fewer. At a given temperature, it seems thus easier to form {111} defects in Ge than in Si. Note that in addition to {111} defects, (001) defects are observed by TEM (45).
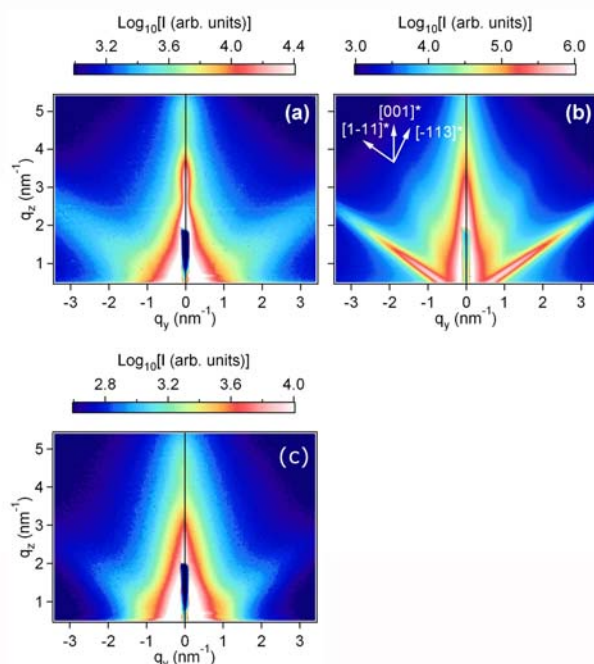

Figure 1: Two dimensional GISAXS patterns of Si or Ge (001) H-implanted at 15 keV, 5×10^{16} cm^{-2}, a) Ge, RT implantation b) Ge, 150°C implantation, c) Si, RT implantation, this sample has been implanted at the same time than the Ge sample in a). q = (q_y, q_z), (q_x = 0) is the scattering vector corrected for refraction effects at the interface air/Ge.

TEM is particularly efficient and complementary to GISAXS to analyse the nanostructure of the defects created during the implantation at different temperatures. The microstructures of the Ge samples implanted at RT and 150°C are compared in Figure 2. As seen, in both cases, the damaged layer can be divided into three zones depending on the defect density and type (31), the highly damaged region (region II) being formed around the maximum of H concentration as calculated by SRIM 2006. As already

revealed by GISAXS experiments, the implantation temperature strongly influences the implantation-induced defects. After a RT implantation only (001), {111} platelets and {113} ribbon-like defects are formed (Figures 2c and d). The typical dimension of these defects is in the tens of nanometer range. When increasing the implantation temperature, the buried layer widens towards the surface (zone Ib in Figure 2b) and other types of H-related extended defects are formed: nanocracks, tiny bubbles, isolated planar clusters of cavities lying in the {111} or (001) planes. Some of the defects are observed at typical stages of their evolution. Figure 2e shows the coalescence of two (001) platelets (see the arrows) which could lead to nanocrack formation during further annealing. Figure 2f reveals the presence of a particular type of defect configuration: four to five bubbles aligned with platelets. In addition, (001) and {111} platelets are observed with typical dimension two or three times higher than those observed after the RT implantation in line with the increase of the GISAXS signal.
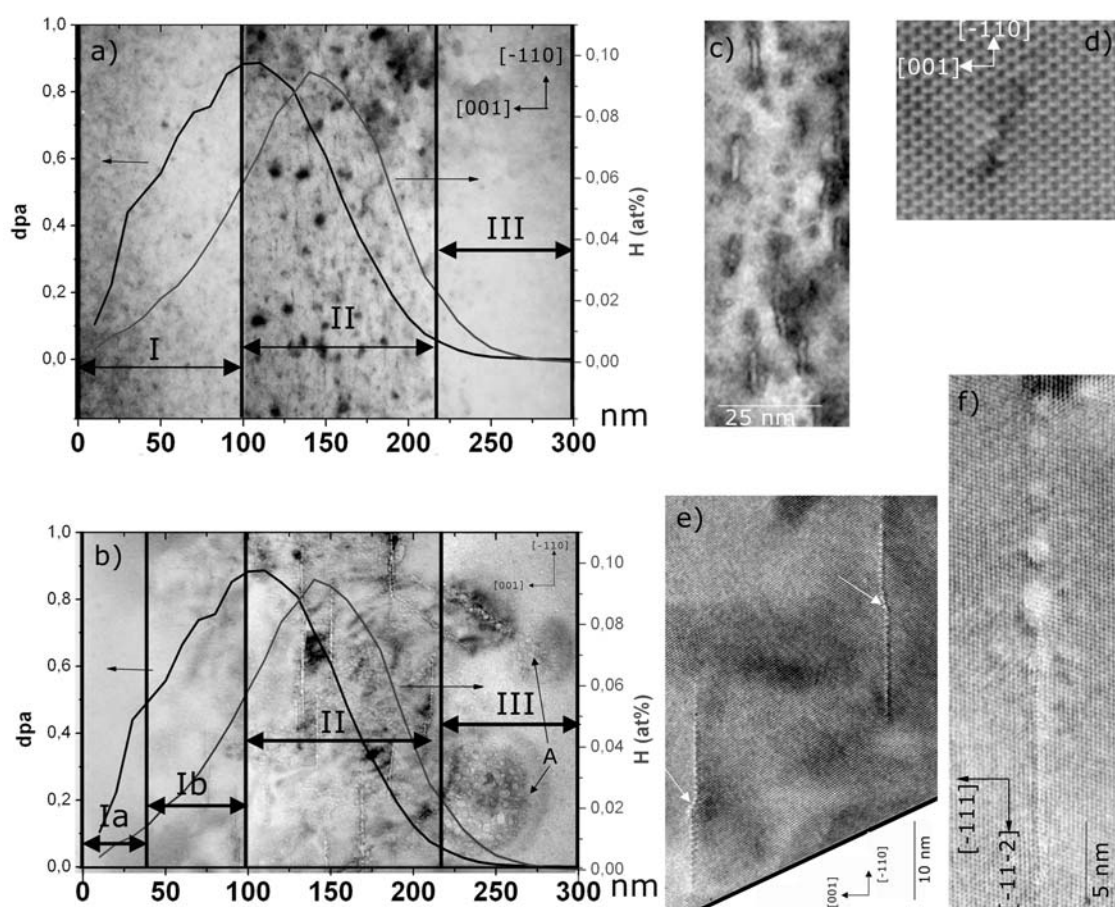

Figure 2: Microstructure of (001) Ge samples implanted with H at 15 keV, 5×10^{16} /cm^2 a) at RT, b) at 150°C, in bright field conditions. The contrast was adapted on the different zones. The displacement per atom (dpa) and H profiles as derived by SRIM06 are superimposed. c) Enlargement of region II of a) in over-focus conditions. d) HRTEM micrograph of a {113} ribbon-like defects after RT implantation. e) HRTEM micrograph showing the coalescence of two (001) platelets after 150°C implantation. f) Platelets and bubbles in the [-11-2] direction after 150°C implantation.

Plasma based ion implantation (PBII)

The influence of the implantation temperature on the defect structure created during implantation is further confirmed by PBII experiments in the range RT-300°C. Three Ge samples have been implanted or annealed under different conditions and then compared. A first sample has been implanted at temperature $T_i \geq 150°C$, another one at $T_i \geq 300°C$, and finally the third one has been implanted at $T_i \geq 150°C$ and annealed at 300°C for 20 min. All the as-implanted Ge samples show a high surface roughness, very likely due to the plasma etching. GISAXS experiments were therefore not suitable and the samples have only been studied by TEM. The microstructures of the three Ge samples are shown in Figure 3. Whatever the implantation and annealing conditions, the damaged region can be divided into two zones depending on the damage density and type (45). As in the case of the conventional implantation, the microstructure is strongly dependent on the implantation temperature. While microcracks, capsules, cylindrical and spherical cavities are observed whatever the implantation and annealing conditions, blisters are only formed for a sufficiently high thermal budget, either during implantation or post-implantation annealing.

Moreover, for $T_i \geq 150°C$, plate-like cavity clusters have been observed in the less damaged region (region II). Their presence is clearly evidenced through tilting experiments. As shown in Figure 4, the cluster appears as a planar arrangement of tiny cavities (less than 1 nm of diameter) when the sample is tilted around the [1-11] or [1-10] directions. Such plate-like cavity clusters, up to 100 nm long, are observed in (001) and {111} planes. As seen in Figure 3c and in its inset, these clusters are still present after an annealing at 300°C, 20 min; however, they appear surrounded by dislocation loops which was not the case before annealing. When increasing the implantation temperature, TEM observations do not reveal any plate-like cavity clusters neither in region II nor in region I.

Finally, (001) and {111} platelets have been observed after PBII whatever the implantation temperature, but these platelets disappear upon annealing at 300°C.
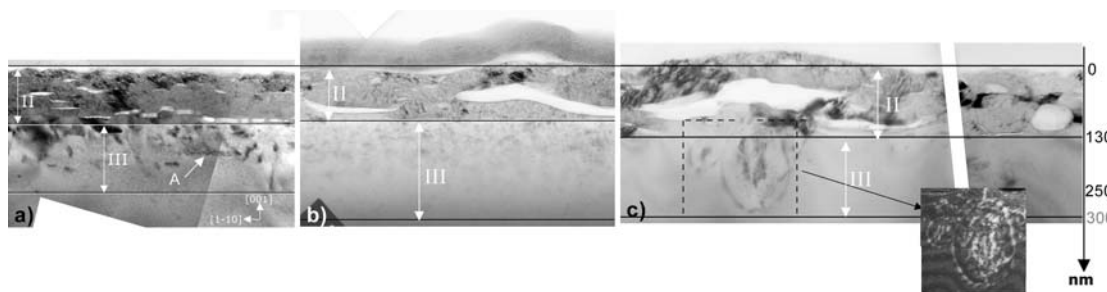

Figure 3: TEM micrographs of (001) Ge samples after PBII of H (20 kV, 5×10^{16} cm^{-2}, 150°C), bright field conditions. a) $T_i \geq 150°C$, b) $T_i \geq 300°C$. The presence of the amorphous layer observed at the top of the implanted sample is for the moment not well understood. c) $T_i \geq 150°C$, followed by an annealing at 300°C, 20 min. In the inset of c), weak beam image of the plate-like cavity clusters surrounded by dislocations.
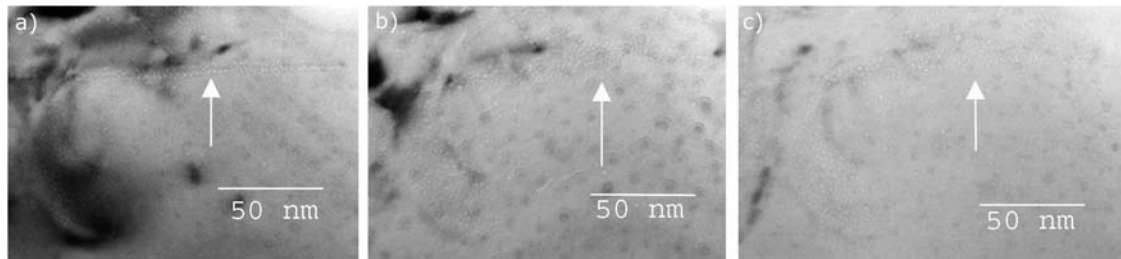
Figure 4: Tilting experiments around the defect labelled A in Figure 3a. a) close to the [110] zone axis. b) tilt around the [1-11] direction. c) tilt around the [1-10] direction.

Helium implantation

The microstructures of Ge samples after He implantation at RT and 200°C are shown in Figures 5a and 5c; as seen, He implantation at RT in Ge leads to the formation of a damaged layer extending from the surface to 850 – 900 nm in depth. This layer contains spherical cavities of about 3 nm of diameter, which often appear to be bounded to dislocations and clusters of point defects mainly distributed between 200 and 600 nm. When increasing the implantation temperature, contrary to H, He implantation leads exclusively to one type of He-related extended defects, spherical cavities, the mean diameter of which has increased up to 7 nm.

In view of a qualitative comparison, results obtained in previous studies on Si (28,29) implanted at RT, 300°C and 400°C are also shown in Figure 5. Obviously, He implantation in Ge leads to about a 1.5 times larger (and deeper) damaged band than in Si. This is rather surprising since the projected range of the 50 keV He ions is about 1.5 times smaller in Ge than in Si. Furthermore, at a given implantation temperature, the mean cavity diameter is not of the same order. However, for instance, the mean cavity diameter of He implanted Ge at 200°C is of the same order of He implanted Si at 400°C, about 7 nm. Thus, in terms of cavity size, He implantation in Si seems to be equivalent to He implantation in Ge but for an implantation temperature at least 200°C higher.
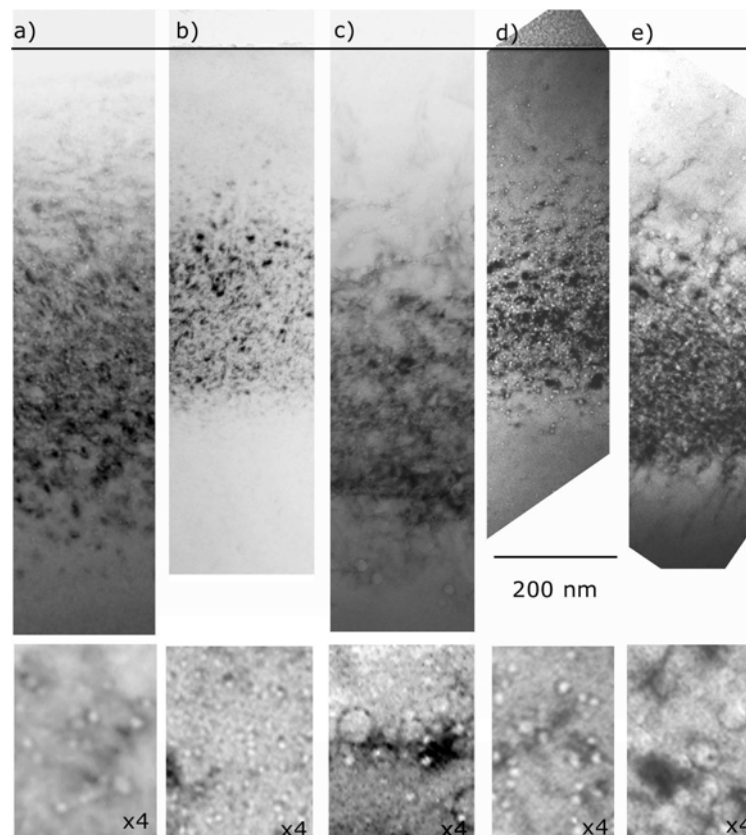
Figure 5: Microstructure of Ge and Si samples implanted with He at 50 keV, 5×10^{16} cm^{-2} and different temperature. a) Ge: RT, b) Si: RT, c) Ge: 200°C, d) Si: 200°C, e) Si: 400°C.

Discussion

As already reported for Si (45), (001) and {111} platelets are readily formed when H is implanted into Ge at RT, suggesting that their formation energies are relatively close. However, their distribution into the damaged band is not random: (001) platelets are located predominantly near R_P whereas {111} platelets form at the deeper side of the buried layer as reported for H-implanted Si (16). In Si, this platelet distribution is explained in terms of strain distribution resulting from the ion implantation (16, 46). The {111} platelets are only formed deeper into the bulk, where the implantation-induced stress is weak. This phenomenon is also observed after plasma hydrogenation in Si, where only variants of {111} platelets are observed (47). This stress-induced orientation has been recently studied in Si where stress was not (or not only) induced by the implantation but rather by a SiGe layer (48) or by He platelets formed before the hydrogenation (49). The symmetry of a previously introduced local strain field can be used to favour platelets orientation variant in Si (49).

The increase of the implantation temperature reduces the lattice damage and therefore the stress and also enhances the mobilities of the different species involved in the extended defect formation. Nucleation and growth of microcracks mostly parallel to the surface are ascribed to the diffusion of molecular hydrogen (H$_2$) towards the platelets resulting in an increase of the internal pressure, and the subsequent mechanical propagation and microcrack formation (45). Cavities are formed as well; they are randomly distributed or arranged in plate-like cavity clusters whereas no cavities at all are observed after RT implantation. This is in good agreement with Raman spectroscopy data

obtained on plasma hydrogenated Ge (38). Intensities of the bands assigned to a stretch local vibrational mode of Ge-H and to free H_2 are found to be dependent on T_i. The Ge-H related signal shows a maximum at RT and then decreases with increasing the substrate temperature to level off at 125°C. On the contrary, the H_2 signal reaches a maximum around 125°C-150°C and decreases with increasing T_i. The increase of the H_2 signal reported in Ref. 38 is assigned to both the formation of cavities and microcracks. Cavity formation has been reported after H implantation in Ge followed by an annealing (37) and plate-like cavity clusters have been observed after plasma hydrogenation at 150°C (50). H_2 is believed to be the ground state of H in Ge (51). From that, Akatsu *et al*. derived that H behaves in Ge similar as aninert gas in Si (37). Indeed, medium or high fluence ($\geq 2x10^{16}$/cm^2) He-implantation in Si leads to the formation of respectively plate-like cavity clusters (52, 53) or a continuous cavity layer (54) whereas platelets are created at low fluence ($1x10^{16}$/cm^2) He implantation (55). In addition, platelet evolution into cavities is reported in RT H-implanted Si after high temperature annealing (56).

The following simplified picture could thus be derived. At RT, atomic H passivates the Ge dangling bonds created by the implantation leading to the platelet formation. For higher implantation temperature, individual H becomes more mobile, increasing the probability of H_2 formation, platelet nucleation being thus in competition with cavity nucleation. Further, the formation of microcracks, larger platelets and of particular configurations as observed in Figure 2e and 2f shows that the temperature is high enough to enhance the defect evolution during the implantation. This is in good agreement with the whole set of defect structures (capsules, cylindrical and spherical cavities) observed after the PBII experiment during which the temperature was higher than 150°C, even if in that case, the high flux used is very likely to be responsible for some of the defect structures. A further increase of the temperature would lead to blistering during the implantation as observed after the PBII experiment at $T_i \geq 300°C$. This shows that the nucleation and growth of extended defects created by H implantation into Ge in the temperature range RT-300°C results from a delicate interplay between kinetic and dynamic effects. The same stands for the temperature range Liquid Nitrogen temperature (LNT)-RT. Indeed, the effect of a RT implantation has been compared with that of an implantation at LNT followed by an "annealing" at RT (33). For a somewhat higher fluence ($6x10^{16}$ cm^{-2}) than that used in the present study, evolved defect structures and blistering have only been observed after the RT implantation showing that strong dynamic evolution can already take place during implantation at RT.

It is worth noting that in the PBII experiments, platelets and plate-like cavity clusters, all located in the less damaged region, exhibit a reverse behaviour with an increase of implantation or annealing temperatures. Indeed, while both defect structures are formed after the PBII at $T_i \geq 150°C$, only platelets are observed when increasing T_i, but they disappear during the annealing at 300°C while the plate-like cavity clusters are still observed. This shows that the plate-like cavity clusters are more stable than platelets during annealing at intermediate temperature but that the dynamic annealing favours platelets rather than plate-like cavity clusters.

Ge and Si have similar properties: diamond structure with bond length of 2.352 Å for Si and 2.450 Å for Ge, indirect bandgap and similar characteristics of isolated H-stabilized defects: the dissociation energy of the Si-H monohydride bond is 2.5 eV whereas it is 1.9 eV for the Ge-H monohydride bond (57, 58). Since much more is known of Si than of Ge, comparison with Si is often useful to explain the behavior of light ion related extended defects in Ge. As it is the case in many respects (59), at the microscopic

level, similar mechanisms are very likely occurring in both materials for the formation of H and He related extended defects. This was pointed out in recent papers concerning H-induced layer transfer or blistering (33, 60) and is further confirmed by this study. For instance, the distribution in depth of (001) and {111} platelets is similar in Ge and Si. However, {111} platelets have been found to be either larger and/or in higher density in Ge than in Si, suggesting that the energy needed to form platelets is smaller in Ge than in Si, in agreement with the threshold fluence for abundant blistering which has been found to be lower in Ge than in Si (1.4 versus 2×10^{16} cm^{-2}) (61).

Moreover, He implantation in Ge at high fluence in the temperature range RT-200°C, leads to the formation of a continuous layer of spherical cavities as in the case of Si. In Ge however, the cavity diameter increases as a function of the implantation temperature. This is in contrast to what has been observed in Si in the same temperature range, where the cavity diameter has been found to stay constant. Indeed, in Si, the RT-300°C range constitutes a first regime during which dynamic annealing leads to a decrease of the cavity density and a stabilization of the cavity diameter (28). The increase of the cavity diameter is only observed in a second regime, between 400°C and 600°C, when the mobility of the different species involved in the cavity formation, is enhanced. This would suggest that, concerning the cavity formation and evolution, similar mechanisms are operating in Ge, only shifted towards lower temperatures. This is in agreement with the conclusions of Desrosiers *et al.* for H implantation in the range LNT-RT (33). It is shown that the evolution of the different types of defects at a given implantation temperature in Ge is similar to that of the corresponding defects in Si for a 100-300°C higher temperature.

The interstitial-type defects observed for a RT H-implantation in Ge and identified as 2D ribbon-like defects tend to follow the scheme described above. They are known as a state of growth under electron irradiation of another type of {113} defects, the 1D rod-like defects (62). Their formation during the TEM experiment could thus not completely be ruled out. However, once focused on a same region of the sample during 30 min, the 300 kV electron beam has not created any ribbon-like defects. Moreover, the {113} defects observed by GISAXS experiments after the 150°C implantation have unambiguously been created by the implantation. High temperature (800°C) He implantation in Si leads to the formation of ribbon-like defects as well. It is ascribed to the dynamical annealing of the first rod-like defects created during the implantation (28). This shows that, under light ion implantation, it is easier to create ribbon-like defects in Ge than in Si.

To summarize, although some discrepancies are observed at the atomic scale (the passivation of cavities seems to be done via monohydrides in Si while it would occur by both monohydrides and dihydrides in Ge (60), available results suggest that at the microscopic level, the average of all the atomic events that lead to the platelet formation and their evolution towards microcracks, is similar in Ge and Si at a temperature normalized with respect to the melt temperature and it seems to be the same for interstitial-related defects.

However, it should be noted that these similarities observed in the case of light ion implantations are no more valid when increasing the ion mass. Indeed, ion implantation in Si leads to the formation of extended defects for a wide range of implantation and annealing conditions but in Ge, except in the case of light ion implantation or electron irradiation, for amorphizing and no-amorphizing Ge$^+$ or Si$^+$ implantations, only dot-like clusters of point defects are observed (68, 69 and reference therein). Further, Posselt *et al.*

(70) have shown that negligible dynamic annealing of defects occurs during Ga implantation in Ge at RT. Moreover, He implantation in Ge leads to a much larger and deeper damaged layer than in Si. This can not be completely explained by a higher mobility of the species involved in the defect formation and is still under investigation.

Conclusion

The effect of the implantation temperature in the range room temperature – 300°C has been studied in hydrogen and helium implanted germanium at high dose and in the energy range of a few tens of keV. The nucleation and growth of extended defects is ascribed to a delicate interplay between dynamic and kinetic effects occurring during the implantation. In the case of He implanted Ge, a continuous cavity layer is formed whatever the implantation temperature in the range studied. The size of the cavities has been found to increase by a factor of 1.5 between implantation at RT and implantation at 200°C.

In many aspects and especially those related to platelets and cavities, it seems that light ion implanted Ge behaves as light ion implanted Si, at temperatures normalized with respect to the melt temperature. The same trends are observed for interstitial related defects; however the discrepancies observed in the width and position of the damaged layer after He implantation show that further investigations are needed.

References

1. M. Bruel, *Electronics Lett.* **31**, 1201 (1995)
2. I. Radu, I. Szafraniak, R. Scholz, M. Alexe and U. Goesele, *J. Appl. Phys.,* **94**, 7820 (2003)
3. Tauzin, A. Akatsu, T. Rabarot, M. Dechamp, J. Zussy, M. Moriceau, H. Michaud, J.F. Charvet, A.M. Di Cioccio, L. Fournel, F. Garrione, J. Faure, B. Letertre and F. Kernevez, *Electronics Lett.,* **41**, 668 (2005)
4. Q.Y. Tong, K. Gutjahr, S. Hopfe, U. Gösele and T.H. Lee, *Appl. Phys. Lett.,* **70**, 1390 (1997)
5. C. Deguet, L. Sanchez, T. Akatsu, F. Allibert, J. Dechamp, F. Madeira, F. Mazen, A. Tauzin, V. Loup, C. Richtarch, D. Mercier, T. Signamarcheix, F. Letertre, B. Depuydt and N. Kernevez, *Electronics Lett.,* **42**, 415 (2006)
6. B. Terreault, *Phys. Stat. Sol. (a),* **204**, 2129 (2007)
7. W. Chen, P. Chen, J.E. Pulsifer, T.L. Alford, T.F. Kuech and S.S. Lau, *Appl. Phys. Lett.,* **92**, 212109 (2008)
8. D. Alquier, C. Bongiorno, F. Roccaforte and V. Raineri, *Appl. Phys. Lett.*, **86**, 21191 (2005)
9. B Hollander, S.T. Lenk, S. Mantl, H. Trinkaus, D. Kirch, M. Luysberg, T. Hakbarth, H.J. Herzog, and P.F.P. Fichtner, *Nucl. Instrum. Methods Phys. Res. B,* **175-177**, 357 (2001)
10. S.M. Myers, G.A. Petersen, D.M. Follstaedt, T.J. Headley, J.R. Michael and C.H. Seager, *Nucl. Inst. Methods Phys. Res. B,* **120**, 43(1996)
11. G.A. Petersen, S.M. Myers and D.M. Follstaedt, *Nucl. Inst. Methods Phys. Res. B* **127/128**, 301 (1997)
12. S.M. Myers and D.M. Follstaedt, *J. Appl. Phys.*, **86**, 3048 (1999)
13. A. Kinomura, Y. Horino, Y. Nakano and J.S. Williams, *J. Appl. Phys.,* **98**, 066102 (2005)

14. V. Raineri, M. Saggio and E. Rimini, *J. Mater. Res.,* **15**, 1449 (2000)
15. S. Personnic, K.K. Bourdelle, F. Letertre, A. Tauzin, N. Cherkashin, A. Claverie, F. Fortunier and H. Klocker*, J. Appl. Phys.,* **103**, 023508 (2008)
16. M. Nastasi, T. Höchbauer, J-K Lee, A. Misra, J.P. Hirth, M. Ridgway and T. Lafford, *Appl. Phys. Lett.* **86**, 154102 (2005)
17. Z. Di, Y. Wang, M. Nastasi, F. Rossi, J.K. Lee, L. Shao and P.E. Thompson, *Appl. Phys. Lett.,* **91**, 244101 (2007)
18. S. Reboh, M.F. Beaufort, J.F. Barbot, J. Grihlé and P.F.P. Fichtner, *Appl. Phys. Lett.,* **93**, 022106 (2008)
19. M.K. Weldon, V.E. Marsico, Y.J. Chabal, A. Agarwal, D.J. Eaglesham, J. Sapjeta, W.L. Brown, D.C. Jacobson, Y. Caudano, S.B. Christman and E.E. Chaban, *J. Vac. Sci. Technol. B*, **15**, 1065 (1997)
20. F.A. Reboredo, M. Ferconi and S.T. Pantelides, *Phys. Rev. Lett.,* **82**, 4870 (1999)
21. S.B Zhang and W.B. Jackson, *Phys. Rev. B,* **43**, 12142 (1991)
22. Yong-sung Kim and K.J. Chang, *Phys. Rev. Lett.* **86**, 1773 (2001)
23. S. Muto, S. Takeda and M. Hirata, *Phil. Mag. A,* **72**, 1057 (1995)
24. N. Martsinovich, M.I. Heggie and C.P. Ewels, *J. Phys.: Condens. Matter* **15**, S2815 (2003)
25. N. Martsinovich, I.S. Martinez and M.I. Heggie, *Phys. Stat. Sol.* **6**, 1771 (2005)
26. S. Hayashi, D. Bruno and S. Goorsky, *Appl. Phys. Lett.,* **85**, 236 (2004)
27. P. Chen, Z. Di, M. Nastasi, E. Bruno, M.G. Grimaldi, N.D. Theodore and S.S. Lau, *Appl. Phys. Lett.,* **92**, 202107 (2008)
28. M.L. David, M.F. Beaufort and J.F. Barbot, *J. Appl. Phys.,* **93**, 1438 (2003)
29. M.L. David, M.F. Beaufort and J.F. Barbot, *Nucl. Inst. Methods Phys. Res. B,* **226**, 531 (2004)
30. D. Babonneau, M.F. Beaufort, A. Declémy, J.F. Barbott and J.P. Simon, *J. Appl. Phys.* **99**, 113507 (2006)
31. M.L. David, F. Pailloux, D. Babonneau, M. Drouet, J.F. Barbot, E. Simoen and C. Claeys, *J. Appl. Phys.,* **102**, 096101 (2007)
32. A. Giguère and B. Terreault, *J. Appl. Phys.* **102**, 106106 (2007)
33. N. Desrosiers, A. Giguère, B. Terreault, M. Chicoine and F. Schiettekatte, *Nucl. Inst. Methods Phys. Res. B*, **266**, 1971 (2008)
34. E. Oliviero, M.L. David, M.F. Beaufort, J. Nomgaudyte, L. Pranevicius, A. Declémy and J.F. Barbot, *J. Appl. Phys.,* **91**, 1179 (2002)
35. E. Oliviero, C. Tromas, F. Pailloux, A. Declemy, M.F. Beaufort, C. Blanchard and J.F. Barbot, *Mater. Sci. and Eng. B*, **102**, 289 (2003)
36. C. Claeys and E. Simoen, *Germanium-Based Technologies: From materials to devices*, Elsevier (2007)
37. T. Akatsu, K.K. Bourdelle, C. Richtarch, B. Faure and F. Letertre, *Appl. Phys. Lett.,* **86**, 181910 (2005)
38. M. Hiller, E.V. Lavrov and J. Weber, *Phys. Rev. B,* **71**, 045208 (2005)
39. D.M. Follstaedt, S.M. Myers and S.R. Lee, *Appl. Phys. Lett.* **69**, 2059 (1996)
40. S.M. Myers, H.J. Stein and D.M. Follstaedt, *Phys. Rev. B* **51**, 9742 (1995)
41. X. Lu, S. Sundar Kumar Iyer, C. Hu and N. W. Cheung, *Appl. Phys. Lett.,* **71**, 2767 (1997)
42. D. Babonneau, S. Peripolli, M.F. Beaufort, J.F. Barbot and J.-P. Simon, *J. Appl. Cryst.,* **40**, s350 (2007)
43. J.F. Ziegler and J.B. Biersack, http://www.srim.org

44. M.L. David, F. Pailloux, M. Drouet, M.F. Beaufort, J.F. Barbot, E. Simoen, C. Claeys, *Sol. Stat. Phenom.,* **131-133**, 103 (2008)
45. M.K. Weldon, V.E. Marsico, Y.J. Chabal, A. Agarwal, D.J. Eaglesham, J. Sapjeta, W.L. Brown, D.C. Jacobson, Y. Caudano, S.B. Christman and E.E. Chaban, *J. Vac. Sci. Technol. B*, **15**, 1065 (1997)
46. J.K. Lee, Y. Lin, Q.X. Jia, T. Höchbauer, H.S. Jung, L. Shao, A. Misra and M. Nastasi, *Appl. Phys. Lett.,* **89**, 101901 (2006)
47. N.M. Johnson, F.A. Ponce, R.A. Street and R.J. Nemanich, *Phys. Rev. B,* **35**, 4166 (1987)
48. Z. Di, Y. Wang, M. Nastasi, F. Rossi, J.K. Lee, L. Shao and P.E. Thompson, *Appl. Phys. Lett.,* **91**, 244101 (2007)
49. S. Reboh, M.F. Beaufort, J.F. Barbot, J. Grihlé and P.F.P. Fichtner, to be published in *Appl. Phys. Lett.*
50. J. Lauwaert, M.L. David, M.F. Beaufort, E. Simoen, D. Depla and P. Clauws, *Mat. Sc. Semicond. Proc.,* **9**, 571 (2006)
51. S.K. Estreicher and D. M. Maric, *Phys. Rev. Lett.,* **70**, 3963 (1993)
52. Oliviero, M.F. Beaufort and J.F. Barbot, J. Appl. Phys. **89**, 5332 (2001)
53. P.F.P. Fichtner, J.R. Kaschny, M. Behar, R.A. Yankov, A. Mücklich and W. Skorupa, Nucl. Inst. Meth. Phys. Res. B **148**, 329 (1999)
54. C.C. Griffioen, J.H. Evans, P.C. De Jong and A. van Veen, Nucl. Instrum. Methods Phys. Res. B, **27**, 417 (1987)
55. C. Macchi, S. Mariazzi, G.P. Karwasz, R.S. Brusa, P. Folegati, S. Frabboni and G. Ottaviani, Phys. Rev. B, **74**, 174120 (2006)
56. J. Grisolia, F. Cristiano, G. Ben Assayag and A. Claverie, Nucl. Inst. Meth. Phys. Res. B, **178**, 160 (2001)
57. S.M. Myers, H.J. Stein and D.M. Follstaedt, *Phys. Rev. B,* **51**, 9742 (1995)
58. S.M. Myers, D.M. Follstaedt, H.J. Stein and W.R. Wampler, *Phys. Rev. B,* **47**, 13380 (1993)
59. J. Vanhellemont and E. Simoen, *Electrochem. Soc. Trans.,* **3**, 451 (2006)
60. J.M. Zahler, A. Fontcuberta I Morral, M.J. Griggs, Harry A. Atwater and Y.J. Chabal, *Phys. Rev. B,* **75**, 035309 (2007)
61. A. Giguère and B. Terreault, *Surf. Coat. Tech.*, **201**, 8205 (2007)
62. C.A. Ferreira Lima and A. Howie, *Phil. Mag.*, **34**, 1057 (1976)
63. S. Takeda, M. Kohyama and K. Ibe, *Phil. Mag. A,* **2**, 287 (1994)
64. D.L. da Silva, P.F.P. Fichtner, A. Peeva, M. Behar, R. Koegler and W. Skorupa, *Nucl. Inst. Methods Phys. Res. B*, **175-177**, 335 (2001)
65. M. Kohyama and S. Takeda, *Phys. Rev B,* **51**, 13111 (1995)
66. S. Rousselet, M.L. David, M.F. Beaufort, J.F. Barbot, A. Declémy, E. Simoen and C. Claeys, to be published.
67. J. Vanhellemont and E. Simoen, *J. Electrochem. Soc.* 154, H572 (2007)
68. E. Simoen, G. Brouwers, A. Satta, M.-L. David, F. Pailloux, B. Parmentier, T. Clarysse, J. Goossens, W. Vandervorst and M. Meuris, submitted to Mat. Sc. Process.
69. D.P. Hickey, Z.L. Bryan, K.S. Jones, R.G. Elliman and E.E. Haller, *J. Vac. Sci. Technol. B* **26**, 425 (2008)
70. M. Posselt, L. Bischoff, D. Grambole and F. Herrmann, *Appl. Phys. Lett.,* **89**, 151918 (2006)